

INTERPLAY OF NEUTRINO OPACITIES IN CORE-COLLAPSE SUPERNOVA SIMULATIONS

ERIC J. LENTZ^{1,2,3}, ANTHONY MEZZACAPPA^{2,1,4}, O.E. BRONSON MESSER^{5,1,4}, W. RAPHAEL HIX^{2,1}, AND STEPHEN W. BRUENN⁶

Accepted for publication to ApJ: 2 Oct 2012

ABSTRACT

We have conducted a series of numerical experiments using spherically symmetric, general relativistic, neutrino radiation hydrodynamics with the code *Agile-BOLTZTRAN* to examine the effects of modern neutrino opacities on the development of supernova simulations. We test the effects of opacities by removing opacities or by undoing opacity improvements for individual opacities and groups of opacities. We find that improvements to electron capture (EC) on nuclei, namely EC on an ensemble of nuclei using modern nuclear structure models rather than the simpler independent-particle approximation (IPA) for EC on a mean nucleus, plays the most important role during core collapse of all tested neutrino opacities. Low-energy neutrinos emitted by modern nuclear EC preferentially escape during collapse without the energy downscattering on electrons required to enhance neutrino escape and deleptonization for the models with IPA nuclear EC. During shock breakout the primary influence on the emergent neutrinos arises from NIS on electrons. For the accretion phase, non-isoenergetic scattering on free nucleons and pair emission by e^+e^- annihilation have the largest impact on the neutrino emission and shock evolution. Other opacities evaluated, including nucleon–nucleon bremsstrahlung and especially neutrino–positron scattering, have little measurable impact on neutrino emission or shock dynamics. Modern treatments of nuclear electron capture, e^+e^- -annihilation pair emission, and non-isoenergetic scattering on electrons and free nucleons are critical elements of core-collapse simulations of all dimensionality.

Subject headings: neutrinos — radiative transfer — supernovae: general

1. INTRODUCTION

As the core of a massive star collapses, electron capture (EC) on protons (free or within nuclei) reduces the electron fraction, Y_e , and releases neutrinos that stream from the core. At densities near $6 \times 10^{11} \text{ g cm}^{-3}$, the mean-free path for neutrinos of mean energy becomes comparable to the size of the core and the neutrinos become “trapped.” The trapping of neutrinos effectively halts the deleptonization (reduction of Y_e) of the core as the emission of neutrinos through EC is balanced by reabsorption of the neutrinos on neutrons (either free or within nuclei). Neutrino opacity regulates the deleptonization and sets the minimum core Y_L (Y_e plus the neutrino fraction, Y_ν), which controls the size of the homologous inner core, $M_{\text{sh}} \propto Y_L^2$ (Yahil 1983). When the density in the core exceeds nuclear density, the nuclear equation of state (EoS) stiffens, and a bounce shock forms at the sonic point that defines the edge of the homologous core. The expanding shock loses energy to neutrino emission and nuclear dissociation and stalls. The neutrino weak interactions (emission, absorption, and scattering) regulate energy loss by the prompt shock to neutrino radiation and thus affect the stalling of the shock.

The revival of the stalled shock by neutrino heating is likewise regulated by the neutrino opacities. As for photons in

stellar atmospheres, we can define “neutrinospheres,” where the neutrinos of each species and energy effectively decouple from the matter in the stellar core. The neutrinosphere radii, R_ν , are dependent on both flavor and energy with R_{ν_e} larger than $R_{\nu_{\mu\tau}}$ because of the increased number of weak interaction channels for ν_e (neutral and charged current). The neutrinosphere radii increase with increasing neutrino energy due to the larger opacities for higher energy neutrinos. The emission temperatures at the various neutrinospheres effectively set the flux of neutrinos in each energy–species group and therefore the spectrum of neutrinos available for absorption in the semi-transparent heating, or “gain,” region between the proto-neutron star and the shock.

Non-isoenergetic scattering (NIS) changes the energy and direction of the neutrinos, each of which plays an important role in all phases of the supernova evolution. Scattering to a lower energy can change the neutrino’s environment from opaque to semi-transparent and allow a neutrino that would otherwise be trapped to escape, both increasing the luminosity of neutrinos available for absorption in the gain region above the core and enhancing lepton escape from the core.

The earliest models of neutrino heating in core-collapse supernovae by Colgate & White (1966) included only emission by electron capture and redeposited half of the energy lost to core neutrino emission in the layers above the proto-neutron star, driving a powerful explosion of the outer layers of the star. Subsequent spherically symmetric models included more detailed treatment of neutrino transport to revive the shock: gray diffusion (Arnett 1966), two-fluid schemes (Hillebrandt et al. 1984; Cooperstein et al. 1986), multi-group flux-limited diffusion (Bruenn 1975; Arnett 1977; Bowers & Wilson 1982; Bruenn 1985; Myra et al. 1987), and Boltzmann transport (Mezzacappa & Bruenn 1993a; Yamada et al. 1999).

The neutrino opacities used evolved in complexity and

elentz@utk.edu

¹ Department of Physics and Astronomy, University of Tennessee, Knoxville, TN 37996-1200, USA

² Physics Division, Oak Ridge National Laboratory, P.O. Box 2008, Oak Ridge, TN 37831-6354, USA

³ Joint Institute for Heavy Ion Research, Oak Ridge National Laboratory, P.O. Box 2008, Oak Ridge, TN 37831-6374, USA

⁴ Computer Science and Mathematics Division, Oak Ridge National Laboratory, P.O. Box 2008, Oak Ridge, TN 37831-6164, USA

⁵ National Center for Computational Sciences, Oak Ridge National Laboratory, P.O. Box 2008, Oak Ridge, TN 37831-6164, USA

⁶ Department of Physics, Florida Atlantic University, 777 Glades Road, Boca Raton, FL 33431-0991, USA

TABLE 1
NEUTRINO OPACITY SUMMARY TABLE

Interaction	Base	Alternate	Model
$\nu e^- \leftrightarrow \nu' e^-$	Schinder & Shapiro (1982)	None	Base-noNES
$\nu e^+ \leftrightarrow \nu' e^+$			Base-noNPS
$\nu n \leftrightarrow \nu' n$	Reddy et al. (1998)	Bruenn (1985)	Base-ISnp
$\nu p \leftrightarrow \nu' p$			
$e^- p \leftrightarrow \nu_e n$	Reddy et al. (1998)	Bruenn (1985)	Base-B85ea-np
$e^+ n \leftrightarrow \bar{\nu}_e p$			
$\nu A \leftrightarrow \nu' A$	Bruenn (1985)	<i>No Change</i>	...
$\nu \alpha \leftrightarrow \nu' \alpha$	Bruenn (1985)	<i>No Change</i>	...
$e^-(A, Z) \leftrightarrow \nu_e(A, Z-1)$	Langanke & Martínez-Pinedo (2000), Langanke et al. (2003)	Bruenn (1985), Fuller (1982)	IPA
$e^+ e^- \leftrightarrow \nu \bar{\nu}$	Schinder & Shapiro (1982)	None	Base-noEPpair
$NN \leftrightarrow NN\nu\bar{\nu}$	Hannestad & Raffelt (1998)	None	Base-noBrems

completeness (Tubbs & Schramm 1975; Lamb & Pethick 1976; Yueh & Buchler 1976; Bludman & van Riper 1978) using the new weak interaction theory (Glashow 1961; Weinberg 1967; Salam 1968) concurrently with relevant experimental results including: the detection of neutral-current interactions in neutrino–nucleon scattering (Hasert et al. 1973) and the discovery of τ^- (Perl et al. 1975), whose neutrino partner, ν_τ , was widely assumed to exist, but was not detected until the turn-of-the-millennium (Kodama et al. 2001).

Schinder & Shapiro (1982) and Bruenn (1985) assembled comprehensive neutrino opacity sets that included energy coupling in the scattering (NIS) and were oriented toward numerical implementation. The Bruenn (1985) opacity set (“B85” hereafter) has been widely adapted both in content and form and has widely served as the “canonical” opacity set. The B85 opacity set includes emission, absorption, and isoenergetic scattering (IS) on heavy nuclei, α -particles, and free nucleons; NIS on electrons; and $\nu\bar{\nu}$ -pair emission from e^+e^- annihilation. (Though derived in Bruenn (1985), NIS on positrons is often omitted from simulations using B85 opacities.)

In the more than 25 years since the compilation of the B85 opacity set, the search for opacity improvements (driven in part, previously, by the possibility that spherically symmetric models might explode if sufficiently detailed) has continued. Some of the newer neutrino channels identified, developed for simulations, and widely adopted include: nucleon–nucleon bremsstrahlung (Hannestad & Raffelt 1998, and a related inelastic ν -nucleon scattering channel); more kinematically complete ν -nucleon emission, absorption, and scattering opacities (Burrows & Sawyer 1998; Reddy et al. 1998); the pair–flavor conversion process (Buras et al. 2003); and tabulated EC rates using ensembles of nuclei with detailed level structures (Langanke et al. 2003; Juodagalvis et al. 2010). Other refinements and corrections to opacities that have been added to many simulations include: weak magnetism for interactions with free nucleons (Horowitz 2002); ion-ion correlations between nuclei (Bowers & Wilson 1982; Horowitz 1997; Itoh et al. 2004); and changes from the effective mass of the nucleons in dense matter (cf., Reddy et al. 1999). For dense matter, from where nuclei become correlated through nuclear matter, the next frontier in the computation of ν -nucleon/nucleus interactions is the development of EoS tables with consistent neutrino opacities for emission, absorption, scattering, and neutrino-pair processes (Reddy et al. 1998; Martínez-Pinedo et al. 2012; Roberts & Reddy 2012).

Updated neutrino opacity sets have been assembled by several authors (Burrows 2001; Buras et al. 2006; Bruenn et al.

2006; Lentz et al. 2012). Prior studies in spherical symmetry have examined the impact of the addition, or modification, of a single opacity (Mezzacappa & Bruenn 1993b; Buras et al. 2003; Messer et al. 2003; Hix et al. 2003; Marek et al. 2005; Langanke et al. 2008) and of multiple, simultaneous, opacity changes in spherical symmetry (Buras et al. 2006; Lentz et al. 2012) and in axisymmetry (2D) (Buras et al. 2006; Müller et al. 2012). This is the first study detailing the effects of each of the opacity changes made to create a modernized opacity set. In this paper, we start from the full set of opacities used in Lentz et al. (2012) and test not only each component of the opacity change in that paper and each opacity upgrade relative to the B85 opacities, but also reexamine the omission of neutrino–electron scattering (NES) and all NIS opacities and omission of each pair-source opacity. In each of our simulations we retain at minimum the B85-formulation of scattering on nucleons and nuclei and emission and absorption on nucleons and nuclei to ensure that the total opacity is not radically changed. While the differences found among the tests of opacity removal are generally consistent with prior single-opacity studies, we find that opacity changes in the context of a detailed opacity set can have different impacts than changing the same opacity in a less complete opacity set. This contextual effect is most prominent for NES during collapse, where the previously identified role of NES in enhancing neutrino escape and core deleptonization during collapse by downscattering neutrinos to lower energies is muted by detailed EC on nuclei. We identify, within our modern opacity set, critical opacities needed for reliable computation of the shock dynamics and neutrino emission during the collapse, shock breakout, and accretion phases, as well as opacities of little impact on the simulation or the observational neutrino properties.

2. NUMERICAL METHODS AND INPUTS

All models in this paper are computed using the parallel version of *Agile*-BOLTZTRAN, a code for general-relativistic, spherically-symmetric, neutrino radiation hydrodynamics (Liebendörfer et al. 2004) with extensions described here.

2.1. *Agile*-BOLTZTRAN

Agile-BOLTZTRAN is a combination of the general-relativistic (GR) hydrodynamics code *Agile* (Liebendörfer et al. 2002) and the neutrino transport code BOLTZTRAN (Mezzacappa & Bruenn 1993a; Mezzacappa & Messer 1999; Liebendörfer et al. 2004). *Agile* solves the complete GR spacetime and hydrodynamics

TABLE 2
MODEL SUMMARY TABLE

Model	Bounce properties				Post-bounce peak	
	Core mass (M_{sh}) M_{\odot}	central ρ_c $10^{14} \text{ g cm}^{-3}$	central Y_e	central Y_L	shock radius km	ν_e -luminosity Bethe s^{-1}
Base	0.430	3.234	0.2448	0.2804	161	408
Base-noNIS	0.431	3.234	0.2453	0.2811	150	478
Base-noNES	0.430	3.234	0.2450	0.2807	158	481
Base-ISnp	0.431	3.233	0.2451	0.2808	153	404
Base-noNPS	0.430	3.233	0.2448	0.2804	160	408
IPA	0.554	3.824	0.2843	0.3331	159	432
IPA-noNIS	0.618	4.239	0.3099	0.3712	148	449
IPA-noNES	0.608	4.162	0.3056	0.3647	159	454
IPA-ISnp	0.554	3.831	0.2849	0.3339	149	430
IPA-noNPS	0.551	3.825	0.2843	0.3331	159	432
Base-noEppair	0.431	3.233	0.2448	0.2804	183	407
Base-noBrems	0.430	3.216	0.2443	0.2798	163	407
Base-noPair	0.435	3.216	0.2443	0.2798	185	410
Base-B85ea-np	0.431	3.239	0.2452	0.2808	159	393

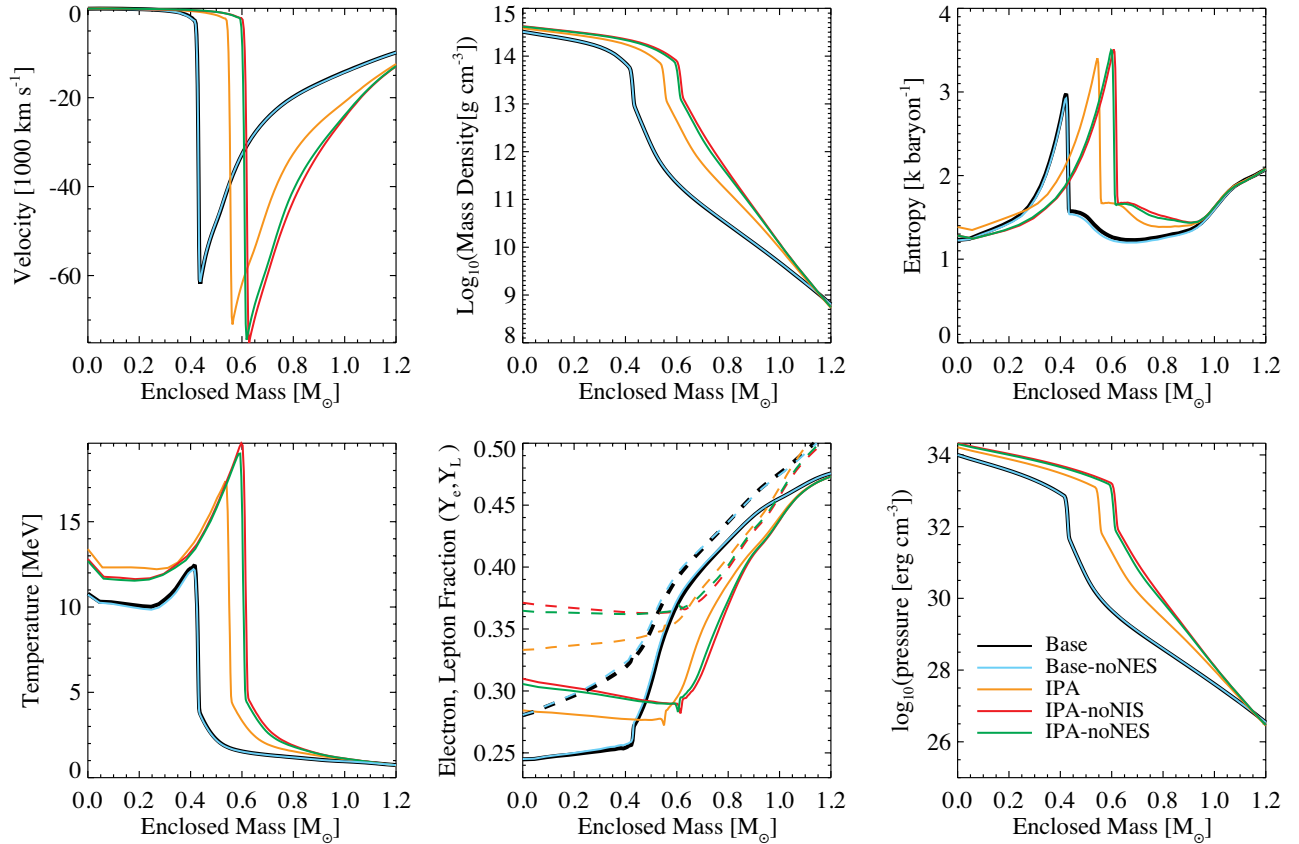


FIG. 1.— Properties of models at core bounce, where bounce is defined as the maximum compression of the central density during the launching of the bounce shock. Models shown are: Base (black; all opacities), Base-noNES (blue; without NES) with the other NIS opacity variation models discussed in Section 3.1.1 indistinguishable from models Base and Base-noNES at bounce and omitted for clarity; the NIS opacity variation models with the IPA EC from Section 3.1.2, IPA (orange; all NIS opacities), IPA-noNIS (red; without NIS opacities; no NES, no NPS, nucleon IS), IPA-noNES (green; without NES), but not IPA-ISnp (nucleon IS), which is indistinguishable from model IPA at bounce and omitted for clarity. The pair opacity test models (Section 3.3) and improved nucleon EC model (Section 3.2) are also indistinguishable from model Base and omitted for clarity. The panels are: radial velocity (upper left), density (upper center), entropy (upper right), temperature (kT , lower left), net electron (or proton) fraction (Y_e , lower center, solid lines), net lepton fraction ($Y_L = Y_e + (n_{\nu_e} - n_{\bar{\nu}_e})/n_{\text{baryons}}$, lower center, dashed lines), and pressure (lower right). All quantities are plotted relative to enclosed rest-mass in M_{\odot} .

equations implicitly in spherical symmetry on a dynamic, moving grid. The moving grid allows us to adequately resolve whole collapsing core, including the shock, using only $\mathcal{O}(100)$ radial zones. Enhancements include the use of a TVD (total variation diminishing) advection scheme in the hydrodynamics solver (Liebendörfer et al. 2005), which improves the accuracy of advection, and the use of δm as the grid coordinate rather than the enclosed mass (Fischer et al. 2010, Section 2.1), which improves numerical accuracy when mass zones are small and density gradients are large. BOLTZTRAN (Mezzacappa & Bruenn 1993a; Mezzacappa & Messer 1999; Liebendörfer et al. 2004) solves the GR neutrino Boltzmann equation using the method of discrete ordinates (S_N) with a Gauss-Legendre quadrature. Here we use an 8-point angular quadrature and 20 logarithmically-spaced energy groups, with group centers from 3 to 300 MeV. The discretization scheme is designed to simultaneously conserve lepton number and energy as described in Liebendörfer et al. (2004). Since we do not include any physics to distinguish between muon- and tau-flavored leptons, we use the combined species $\nu_{\mu\tau} = \{\nu_\mu, \nu_\tau\}$ and $\bar{\nu}_{\mu\tau} = \{\bar{\nu}_\mu, \bar{\nu}_\tau\}$.

2.2. Opacities and other inputs

For all models we use the nuclear, electron, and photon equations of state (EoS) of Lattimer & Swesty (1991) with the bulk incompressibility of nuclear matter $\kappa_s = 220$ MeV.⁷ This matches the current experimental value of $\kappa_s = 240 \pm 20$ MeV (Shlomo et al. 2006) better than the value of 180 MeV more commonly used with LS EoS in the past, though the value of κ_s has been shown to be of little consequence during the early phases of core-collapse supernova evolution shown here (Swesty et al. 1994; Thompson et al. 2003; Lentz et al. 2010). Matter outside the “iron” core⁸ is treated as an ideal gas of ^{28}Si that “flashes” instantaneously to nuclear statistical equilibrium when the temperature exceeds $kT > 0.47$ MeV.

The stellar progenitor used for all models reported here is the 15- M_\odot solar-metallicity progenitor of Woosley & Heger (2007). We have mapped the inner 1.8 M_\odot of the progenitor onto 108 mass shells of the adaptive radial grid.

The base opacity set includes emission, absorption, and scattering on free nucleons (Reddy et al. 1998); isoenergetic scattering on heavy nuclei and α -particles (Bruenn 1985); scattering of neutrinos on electrons (NES) and positrons (NPS) (Schinder & Shapiro 1982); production of neutrino pairs from e^+e^- annihilation (Schinder & Shapiro 1982) and nucleon-nucleon bremsstrahlung (Hannestad & Raffelt 1998); and electron capture (EC) on nuclei using the LMSH EC table of Langanke et al. (2003), which utilizes the EC rates of Langanke & Martínez-Pinedo (2000) and Sampaio et al. (2002). The full angle and energy exchange for scattering between the neutrinos and electrons, positrons, and nucleons is included, while scattering on nuclei is isoenergetic. Bremsstrahlung and e^+e^- annihilation are the only sources of $\nu_{\mu\tau}$ and $\bar{\nu}_{\mu\tau}$.

In this paper we conduct numerical experiments where individual opacities in the modernized base set are replaced with alternatives, or removed. For NES, NPS, and the e^+e^-

annihilation and bremsstrahlung pair sources we have no alternatives so these opacities are tested by removal. For emission, absorption, and scattering on nucleons, and EC on nuclei, the base opacity components are replaced individually by the simpler versions in Bruenn (1985). The alternative to the LMSH EC table, which includes detailed emission rates over an ensemble of nuclei, is an independent particle approximation (IPA) (Fuller 1982; Bruenn 1985), which cuts off when the mean neutron number of the heavy nuclei $N \geq 40$. The alternative to the NIS nucleon scattering opacities of Reddy et al. (1998) are the more approximate IS equivalents from Bruenn (1985), which include the phase space, but not the recoil of the nucleons. The alternative to the neutrino emission and absorption on free nucleon opacities of Reddy et al. (1998) from Bruenn (1985) uses an approximate phase space factor and omits nucleon recoil effects. Ion-ion correlations and weak magnetism are omitted from our opacity set and tests. The scattering on nuclei remains the Bruenn (1985) form for all models. The base opacities and their alternatives along with the models testing each alternative are summarized in Table 1.

3. RESULTS

A previous paper (Lentz et al. 2012) examined the effects of removing significant sections of the available modern opacity set with noticeable consequences. However, the effects of individual opacity changes were not isolated and the opacity comparison was conducted using Newtonian hydrodynamics and gravity and $\mathcal{O}(v/c)$ transport. In this paper we start from the same general relativistic model with the full modern opacities and examine the effects of the various opacities in detail. The tests are organized into three groups: 1) non-isoenergetic scattering opacity tests, 2) emission/absorption opacity tests, and 3) pair opacity tests. Each modern opacity is removed or replaced with an alternative, individually, with additional models in which groups of opacities are removed or replaced with alternatives. The models are summarized in Table 2. The configurations at bounce of all distinguishable models are plotted in Figure 1. We limit our simulations to the first 150 ms after bounce when shock radius, proto-neutron star radius, and thermodynamic profiles are reasonable approximations to multi-dimensional models.

3.1. Non-isoenergetic Scattering Comparisons

There is a rich literature (Bruenn 1985; Bruenn & Haxton 1991; Mezzacappa & Bruenn 1993b; Smit et al. 1996; Thompson et al. 2003) on NES effects in core-collapse demonstrating that, despite being a relatively small contributor to the total scattering opacity, neutrino-electron scattering (NES) plays an important role in determining core deleptonization during collapse. The dominant opacities that control the flow of neutrinos and lepton number from the core are energy dependent, with larger opacities (lower mean free paths) for higher neutrino energies. Energy downscattering by neutrinos on electrons (or other constituents) lowers the energy and therefore the optical depth of the scattered neutrino. This opens a natural channel for enhanced neutrino escape that is artificially suppressed when NIS opacities are excluded from the core-collapse model.

We retest the effects of energy downscattering on collapse and the subsequent evolution of the collapsed core by removing each source of NIS individually from our reference model Base. We also compare to a model that includes no NIS opacities. Surprisingly, given the previous studies, none

⁷ We use the latest version of the Lattimer & Swesty (1991) EoS, version 2.7, which is available for download from its authors at <http://www.astro.sunysb.edu/dswesty/lseos.html>.

⁸ The Fe-core is defined as the inner core that is in nuclear statistical equilibrium (NSE) or where the mass fraction of Fe-peak nuclei exceeds 0.5.

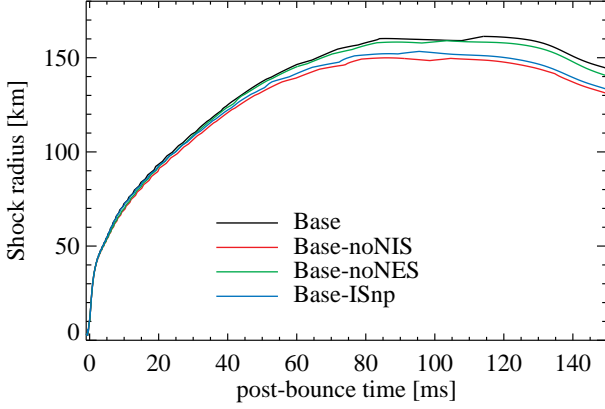


FIG. 2.— Shock trajectories in km, versus time after bounce, for all models in Section 3.1.1. The models plotted are Base (black; all opacities included), Base-noNIS (red; without NIS opacities; no NES, no NPS, nucleon IS), Base-noNES (green; without NES), and Base-ISnp (blue; nucleon IS). Shock position is computed by bisecting the pair of mass shells with the largest negative radial velocity gradient $-\partial v_r / \partial r$.

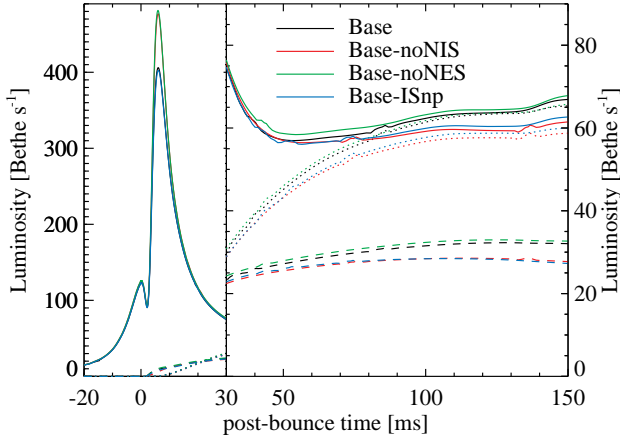


FIG. 3.— Comoving-frame neutrino luminosities measured at 400 km for all models in Section 3.1.1. Colors are as in Figure 2. Electron neutrino, ν_e , luminosities are represented by solid lines, $\bar{\nu}_e$ -luminosities by dotted lines, and $\nu_{\mu\tau}$ -luminosities by dashed lines. For the heavy lepton flavor neutrinos, $L_{\mu\tau} \equiv L_\mu = L_\tau$, is the luminosity of a single species and not a sum. $\bar{\nu}_{\mu\tau}$ -luminosities are indistinguishable from $\nu_{\mu\tau}$ -luminosities, and omitted from this figure. The luminosities are in Bethe s^{-1} , where 1 $\text{Bethe} = 10^{51}$ ergs.

of these changes affected the collapse phase, though differences do emerge after core bounce (Section 3.1.1). To sort out these differences, we repeated the full set of numerical experiments after removing a key opacity unavailable in the previous studies—the LMSH electron capture table. The results using the IPA EC (Section 3.1.2) follow the general expectations of the previous studies. The analysis of the difference made by the choice of EC opacity during collapse (Section 3.1.3) provides a cautionary warning about the coupled nature of the neutrino opacity contributions to collapse and the viability of explosions.

3.1.1. NIS comparisons using LMSH EC table

For this set of tests we compare a model with our full opacity set (Base) to models without electron scattering (Base-noNES), without positron scattering (Base-noNPS), replacing the nucleon scattering of Reddy et al. (1998) with the IS equivalent of Bruenn (1985) (Base-ISnp), and to a model with all three of these changes (Base-noNIS). *At bounce we find no*

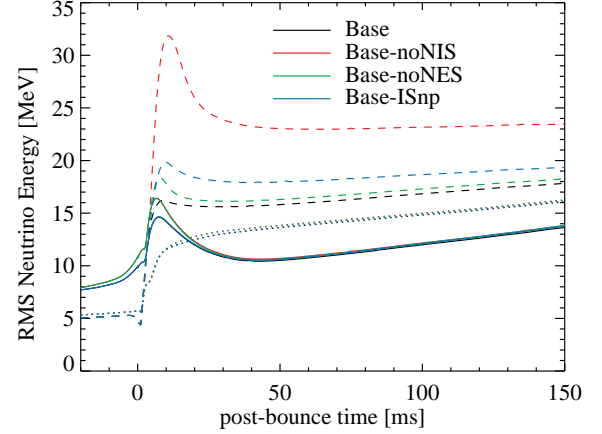


FIG. 4.— Comoving-frame neutrino RMS energies, $\langle E_\nu \rangle_{\text{RMS}} = (\int d\mu dE E^4 F / \int d\mu dE E^2 F)^{1/2}$, measured at 400 km for all models in Section 3.1.1. RMS energy is computed over number density, not number flux. Colors are as in Figure 2. Line styles are as in Figure 3.

noticeable differences among the models. (See Figure 1 and Table 2.) As the shock reaches its largest extent (Figure 2), two splittings are visible. (The model without positron scattering, Base-noNPS, is omitted from the plots and discussion as it is indistinguishable from the Base model.) The smaller splitting reaching 2–3 km by ≈ 80 ms post-bounce is created by omitting electron scattering. The larger splitting, originating at ≈ 30 ms post-bounce, is 10–15 km and is created by replacing the NIS nucleon scattering with the IS equivalent. In both cases, the larger radius is obtained by the model with more NIS opacity. The splitting in the shock radii is reflected in the luminosities for the same epoch (Figure 3). The choice of nucleon scattering opacity makes the largest difference, with the nucleon NIS-containing models (Base, Base-noNES) having larger luminosities for all neutrino species, ≈ 5 –6 Bethe s^{-1} for each species at 150 ms after core bounce, due to smaller total scattering opacity for the nucleon NIS of Reddy et al. (1998) than the nucleon IS of Bruenn (1985), permitting easier escape of trapped $\nu_e \bar{\nu}_e$ from the core. A much smaller difference in luminosities exists for the omission of NES. The larger ν_e - and $\bar{\nu}_e$ -luminosities for models using the NIS nucleon scattering sustain larger shock radii through higher gain-region net heating rates. For the smaller splitting in luminosity and shock radius due to removing NES, the correlation between luminosity and shock radius is weaker, being inverted in the case including nucleon NIS. We were unable to isolate a cause for this small difference. For the two models using nucleon IS, the model with NES (Base-ISnp) has slightly higher luminosity and shock radius than the model without NES (Base-noNIS); but, for the two models with nucleon NIS, the model with NES (Base) has *lower* luminosity and higher shock radius relative to the model without NES (Base-noNES). ? have proposed an analytic proportionality for the shock radius, $R_{\text{sh}} \propto (L_\nu \langle E_\nu^2 \rangle)^{4/9} R_{\nu s}^{16/9}$, where $R_{\nu s}$ is the neutrinosphere radius. If we consider only the effect of $\nu_e \bar{\nu}_e$ -luminosity we would find a relation closer to $R_{\text{sh}} \propto L_\nu$ for the scattering models showing larger differences in luminosities in this section and Section 3.1.2, indicating that the increase in neutrinosphere radii from lower opacities (for the more luminous models) are also playing a role in the shock radius. There are no detectable differences among these models in the $\langle E_{\nu_e} \rangle_{\text{RMS}}$ and $\langle E_{\bar{\nu}_e} \rangle_{\text{RMS}}$ (Figure 4) during the accretion epoch. During the accretion phase, the various neutri-

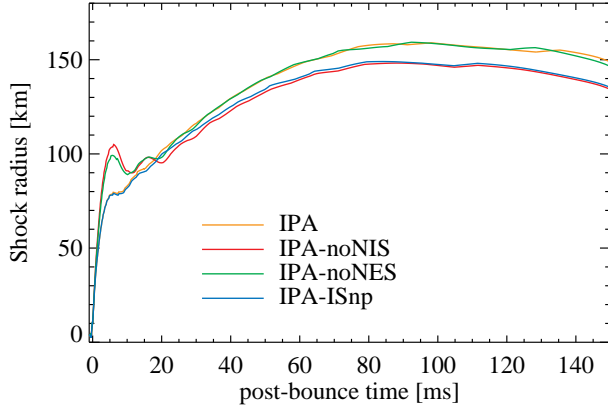


FIG. 5.— Shock trajectories in km, versus time after bounce, for all models in Section 3.1.2. Models are IPA (orange; all NIS opacities), IPA-noNIS (red; without NIS opacities; no NES, no NPS, nucleon IS), IPA-noNES (green; without NES), and IPA-ISnp (blue; nucleon IS).

nospheres and the entire gain region are within a gas composed primarily of electrons and free protons and neutrons, and the nucleon scattering opacity improvements are reflected in the radiation and hydrodynamic quantities. In addition to permitting non-isoenergetic scattering, the improved nucleon opacities account for nucleon phase blocking, recoil, etc., which also make modest alterations to the total scattering opacity.

During breakout we see a different behavior, with NES being the more important NIS opacity. The breakout burst L_{ν_e} is approximately 480 Bethe s^{-1} for models without NES (Base-noNES, Base-noNIS) and approximately 405 Bethe s^{-1} for models with NES (Base, Base-ISnp). The same grouping applies for $\langle E_{\nu_e} \rangle_{\text{RMS}}$, which is up to 2 MeV higher during breakout and up to 1 MeV higher before bounce for models without NES. The breakout burst represents the passage of the shock through the neutrinospheres, and the material above the shock is primarily composed of heavy nuclei. Therefore, scattering on free nucleons is of less importance to the neutrino spectrum during breakout. The electrons above the shock downscatter the energies of the escaping neutrinos and lower the $\langle E_{\nu_e} \rangle_{\text{RMS}}$ and, therefore, the total luminosity.

The most dramatic difference seen in these models is in the quantity $\langle E_{\nu_{\mu\tau}} \rangle_{\text{RMS}}$ (Figure 4, dashed lines), with significant differences across all the models. At 150 ms post-bounce the increase in $\langle E_{\nu_{\mu\tau}} \rangle_{\text{RMS}}$ relative to the Base model is approximately 0.5 and 1.5 MeV, respectively, for models Base-noNES and Base-ISnp, while the increase is nearly 7 MeV for model Base-noNIS, with all NIS scatterings removed. This demonstrates the non-linear nature of the opacity changes. Energy lost by $\nu_{\mu\tau}$ via scattering thermalizes the spectra of $\nu_{\mu\tau}$ reducing $\langle E_{\nu_{\mu\tau}} \rangle_{\text{RMS}}$ and serves as an important source of heating between the $\nu_{\mu\tau}$ - and ν_e -neutrinospheres. (See Section 3.3 for further discussion.) In model Base-noNIS there are no scattering processes remaining to thermalize the spectrum of $\nu_{\mu\tau}$ after emission. NIS from either nucleons or electrons is enough to significantly lower $\langle E_{\nu_{\mu\tau}} \rangle_{\text{RMS}}$, with both required for the full effect. The lack of variation in $\langle E_{\nu_e \bar{\nu}_e} \rangle_{\text{RMS}}$ after breakout for these models demonstrates that absorption followed by emission plays the role of an “effective downscattering” in thermalizing the neutrino spectra.

3.1.2. NIS comparisons using IPA EC

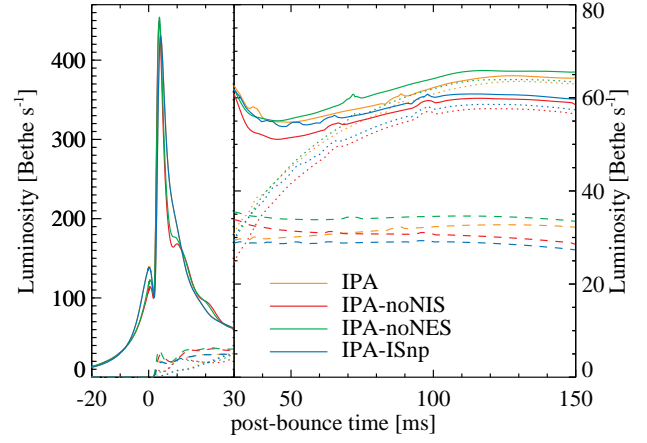


FIG. 6.— Comoving-frame neutrino luminosities measured at 400 km for all models in Section 3.1.2. Colors are as in Figure 5. Line styles are as in Figure 3. The luminosities are in Bethe s^{-1} , where $1 \text{ Bethe} = 10^{51} \text{ ergs}$.

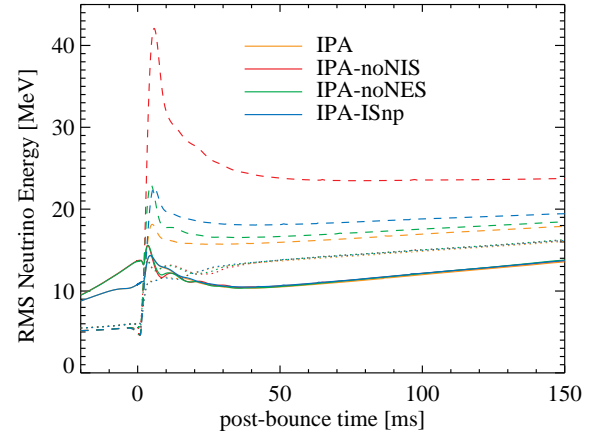


FIG. 7.— Comoving-frame neutrino RMS energies measured at 400 km for all models in Section 3.1.2. Colors are as in Figure 5. Line styles are as in Figure 3.

The lack of effects at bounce from reduced NIS opacities stands in contrast to the results of Mezzacappa & Bruenn (1993b) who used an earlier version of our code with the same NES opacity. Therefore, we repeated our NIS subtraction experiments with the LMSH EC table replaced by the IPA EC of Bruenn (1985) that Mezzacappa & Bruenn (1993b) used. The replacement of the LMSH EC table with the IPA EC has the largest effect on the bounce configuration of any pair or emission/absorption opacity alternatives. (See Figure 1. Those differences will be discussed individually in Sections 3.2 and 3.3.) At core bounce (Figure 1), the primary differences among these models are attributed to the inclusion or omission of NES. The homologous core mass, M_{sh} , shifts from $0.544 M_{\odot}$ for model IPA with all NIS opacities, to $0.608 M_{\odot}$ for model IPA-noNES with NES removed. There is a slightly larger shift in M_{sh} to $0.618 M_{\odot}$ for model IPA-noNIS without the remaining NIS opacities. (The model without NPS, IPA-noNPS, is indistinguishable from the model IPA throughout and is omitted from the plots and discussion.) Correlated to the increase in M_{sh} is Y_L , which increases from 0.333 for IPA to 0.365 for IPA-noNES. There is a corresponding increase in Y_e from 0.284 to 0.306 and in net neutrino number, $Y_{\nu} = Y_L - Y_e$, from 0.0488 to 0.0591, consistent with the effects of NES described by Mezzacappa & Bruenn (1993b), where scattering by NES moved neutrinos to lower

energies with lower opacities and an easier path to escape. In the models without NES, neutrinos are not scattered to lower energies by electrons, and are not aided in their escape. During collapse, the core consists primarily of heavy nuclei and electrons, therefore NIS on free nucleons has little effect, as we can see from these models. The model with nucleon IS and including NES, IPA-ISnp, is indistinguishable from model IPA at bounce. The models with higher core Y_e have a correspondingly higher core density, pressure, and post-shock temperature.

During breakout, the inclusion or omission of NES remains the primary difference among the models. The shocks (Figure 5) for these models with the IPA EC on nuclei launch more vigorously and from shallower depths in the gravitational well than the shocks for the LMSH EC models (Figure 2). The vigor of these launched shocks creates a slight oscillation in shock radius for the models with NES (IPA, IPA-ISnp) and a prominent shock “ringing” in the models without NES (IPA-noNES, IPA-noNIS), also seen by Thompson et al. (2003) for a model without NES. The breakout luminosity for ν_e peaks somewhat higher at $L_{\nu_e} \approx 450 \text{ Bethe s}^{-1}$ for the models without NES and $\approx 430 \text{ Bethe s}^{-1}$ for the models that include NES. (See Table 2.) The breakout burst luminosity in ν_e also drops faster for the models without NES and exhibits oscillations in all luminosities and $\langle E_\nu \rangle_{\text{RMS}}$ (Figure 7). The RMS energies for ν_e are also higher in the pre-bounce phase for the models without NES. During breakout the shock passes through the various ν_e -neutrinospheres, and in the case of the models without NES, the shock oscillates through the neutrinospheres.

At 20 ms after bounce the shock trajectories cross (Figure 5) and by 40 ms after bounce the primary difference between models is the use of NIS or IS nucleon opacities. Like for the models with the LMSH table, the shock radius in the later epochs is $\approx 10\text{--}12 \text{ km}$ larger for models using the nucleon NIS of Reddy et al. (1998) (IPA, IPA-noNES) than those using the nucleon IS of Bruenn (1985) (IPA-ISnp, IPA-noNIS). Within these pairs of models and during this epoch, the difference caused by NES is even smaller for the IPA EC models than the LMSH EC models. This difference in shock radii is also reflected in the luminosities (Figure 6), with larger luminosities for models with nucleon NIS than for those with nucleon IS. Lower scattering opacity for nucleon NIS again enhances escape of trapped $\nu_e \bar{\nu}_e$, increasing their luminosities, the heating from absorption, and the shock radius. The smaller shifts in luminosity within these nucleon scattering pairs due to their differences in the inclusion or omission of NES are not reflected in the shock radii.

The late-time behavior of $\langle E_\nu \rangle_{\text{RMS}}$ (Figure 7) for these IPA EC models is similar to the LMSH EC models. After $\approx 40 \text{ ms}$, differences in $\langle E_{\nu_e} \rangle_{\text{RMS}}$ and $\langle E_{\bar{\nu}_e} \rangle_{\text{RMS}}$ are undetectable for these models. The peak $\langle E_{\nu_{\mu\tau}} \rangle_{\text{RMS}}$ (dashed lines) during breakout changes from 18 MeV for model IPA with all NIS opacities included, to approximately 23 MeV for the two models with one NIS opacity missing (IPA-noNES, IPA-ISnp), to 42 MeV for model IPA-noNIS with all NIS opacities omitted. For the IPA-noNIS model, there are no energy-exchanging scatterings to alter the spectrum, and what we see is the emission spectra of all emitted neutrinos integrated over the semi-transparent pair-emitting region. Inclusion of either NES or nucleon NIS is enough to push the observed $\nu_{\mu\tau}$ -spectrum most of the way toward the values in model IPA with all of the NIS opacities. A similar effect is also seen

at 150 ms after bounce when the models with one missing NIS opacity (IPA-noNES, IPA-ISnp) have $\langle E_{\nu_{\mu\tau}} \rangle_{\text{RMS}}$ that is $< 2 \text{ MeV}$ larger than for the IPA model, while for the model without any NIS opacities (IPA-noNIS), $\langle E_{\nu_{\mu\tau}} \rangle_{\text{RMS}}$ is 6 MeV larger than for model IPA, demonstrating the non-linear interplay of the NIS opacities on the thermalization of the $\nu_{\mu\tau} \bar{\nu}_{\mu\tau}$ spectra.

3.1.3. Interaction between NIS and EC during collapse

To illustrate the interplay between nuclear electron capture and non-isoenergetic scattering during collapse, we plot the occupation number (where values of 1 represent a completely occupied phase-space) of ν_e as a function of energy, the zeroth moment of the distribution function, for three pre-bounce epochs. In Figure 8 we compare the spectra of models with the LMSH EC (Base, Base-noNIS; black lines) to models using the IPA EC (IPA, IPA-noNIS; orange lines), for both cases: including the full set of NIS opacities (Base, IPA; solid lines) and omitting all NIS opacities (Base-noNIS, IPA-noNIS; dashed lines). During collapse the central density, ρ_c , serves as a useful “clock” for comparing different models, and the spectra are plotted for $\rho_c = 10^{11}, 10^{12}$, and $10^{13} \text{ g cm}^{-3}$ (top, middle, and bottom panels, respectively). At $\rho_c = 10^{11} \text{ g cm}^{-3}$ (upper panel) the spectra are relatively similar, though the IPA EC models have fewer neutrinos at low energies and slightly more neutrinos in the high-energy tail. At $\rho_c = 10^{12} \text{ g cm}^{-3}$ (center panel) there is a clear separation between the models. The overall phase-space occupation has increased for all models, though for the lowest energy neutrinos in model IPA-noNIS, it has only slightly increased. The high-energy tail for the IPA EC models (orange lines) is shifted $\approx 40\text{--}50\%$ higher in energy relative to the LMSH EC models (black lines), with the model lacking NIS, IPA-noNIS, having the largest shift. At energies less than $\approx 15 \text{ MeV}$, model IPA-noNIS has fewer neutrinos than the other models, approximately 30 times fewer for the lowest-energy neutrinos. Unlike the other models, which have fairly flat neutrino spectra up to the high-energy roll-off, model IPA-noNIS has a peak at 20 MeV. At $\rho_c = 10^{13} \text{ g cm}^{-3}$ (lower panel) the trend continues with model IPA-noNIS as the outlier. The high-energy tail of the ν_e -spectrum for IPA EC models (orange lines) is again shifted $\approx 40\text{--}50\%$ in energy relative to the LMSH EC models (black lines) with a smaller shift for models without NIS (dashed lines) relative to those with NIS (solid lines). The neutrino phase-space is (nearly) completely filled for $E < 20 \text{ MeV}$ for the LMSH EC models (black lines) and for $E < 30 \text{ MeV}$ for model IPA, while model IPA-noNIS reaches a peak at 30 MeV and decreases for lower energies. The spectra for the IPA EC models (Figure 8, orange lines) are consistent with previously reported collapse-phase spectra (Bruenn 1985; Smit et al. 1996).

In the independent particle approximation, nuclear EC is completely shut-off when the mean neutron number $N > 40$, which occurs at densities above $\approx 2 \times 10^{10} \text{ g cm}^{-3}$, constituting much of the core collapse. Therefore, in the IPA EC models (IPA, IPA-noNIS) all of the ν_e emission in regions with density exceeding $\approx 2 \times 10^{10} \text{ g cm}^{-3}$ arises from electron capture on free protons, which are relatively rare, and results in a slower overall rate of ν_e emission and core deleptonization. (Pair emission is correspondingly low during collapse as we shall discuss in Section 3.3.) The LMSH EC implementation emits neutrinos with a lower mean energy than the capture on protons, which dominates the total capture rate in the IPA models at densities above $\approx 2 \times 10^{10} \text{ g cm}^{-3}$,

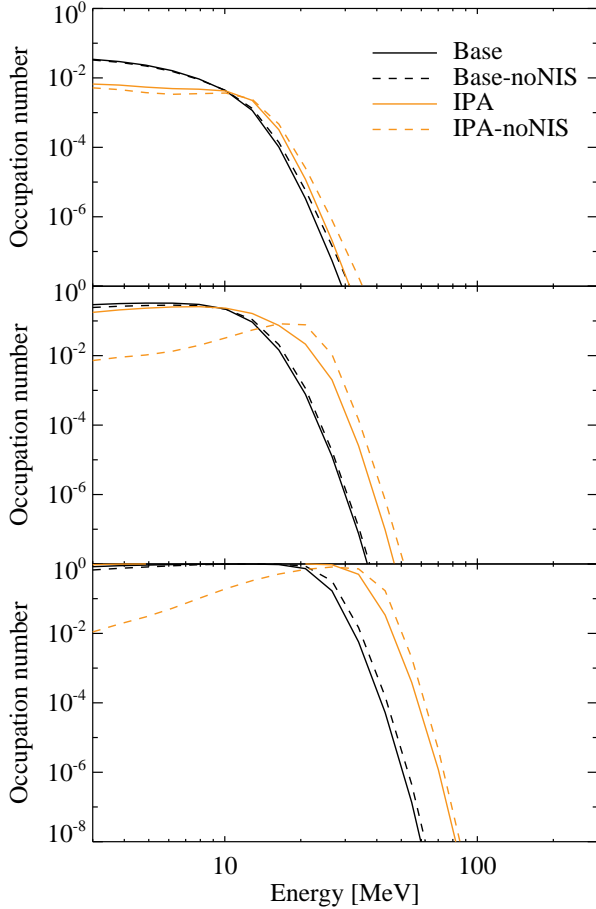


FIG. 8.— Spectral neutrino occupation number (zeroth angular moment of the invariant neutrino distribution function) versus comoving-frame neutrino energy at mass shell $M = 0.25 M_{\odot}$ for the models discussed in Section 3.1.3. The models are Base (black, solid), Base-noNIS (black, dashed), IPA (orange, solid), and IPA-noNIS (orange, dashed). The three panels are for the models at central densities, ρ_c , of $1 \times 10^{11} \text{ g cm}^{-3}$ (upper panel), $1 \times 10^{12} \text{ g cm}^{-3}$ (middle panel), and $1 \times 10^{13} \text{ g cm}^{-3}$ (lower panel).

and fills the low energy spectra which is underpopulated by EC on protons (Langanke et al. 2003), which we can see by comparing the spectral evolution of the models without NIS opacities for the LMSH EC (Base-noNIS) and IPA EC (IPA-noNIS). With IPA EC, the low-energy spectrum can only be filled by energy downscattering by NIS opacities, which efficiently fill the low-energy spectrum for model IPA. Using the LMSH EC fills the low-energy ν_e spectrum directly without energy downscattering (model Base-noNIS), so we do not see an enhancement in neutrino escape through the less opaque neutrino “window” at lower energies when NIS opacities are included, like we do for the IPA EC models.

Scattering on nuclei is the dominant contributor to total opacity during collapse and identical in all of our models. Once the low-energy phase space is filled, deleptonization is controlled by the total opacity, and thus there are no discernible differences in the deleptonization among the LMSH EC models presented in Section 3.1.1. For the IPA EC models presented in Section 3.1.2, changes to the filling of the low-energy phase space, do affect the net escape after trapping

begins. The differences between the models with the full set of NIS opacities (Base, IPA) are a consequence of differences in EC before trapping occurs (Hix et al. 2003).

After considering the effects of compression due to variation in central density on the temperature and the change in entropy profiles due changes in M_{sh} among the models plotted in Figure 1, there is likely an additional small increase in temperature and entropy inside the shock for models that include IPA EC and NES (orange lines). This small thermal increase is likely due to energy gained by the fluid from the scattering of ν_e by electrons as can be seen in difference between the model IPA and model IPA-noNIS spectra in Figure 8. The lack of similar effects on the entropy and temperature by changes in scattering on models using the LMSH EC, suggests (as does the lack of impact on the spectra during collapse) that the NIS has very little impact on ν_e during collapse when utilizing the more complete LMSH EC implementation.

3.2. Emission and absorption comparisons

To test the two sources of ν_e ($\bar{\nu}_e$) emission via electron (positron) capture and the inverse neutrino absorption in the modern opacity set of model Base, we replaced them with their Bruenn (1985) equivalents for EC on nuclei (model IPA) and EC on free nucleons (model Base-B85ea-np). At bounce (Figure 1), the change in nucleon EC produces no discernible difference between models Base and Base-B85ea-np, but changing the nuclear EC produces the largest differences at bounce of any single opacity replacement tested in this paper. As noted by Hix et al. (2003), the IPA EC (model IPA) results in less deleptonization, as the IPA turns off completely where the heavy nuclei have neutron numbers $N \geq 40$, of the inner core relative to using the LMSH EC (model Base) leading to higher Y_e , Y_L , density, pressure, and temperature inside the bounce shock. The IPA EC also results in higher deleptonization and stronger collapse *outside* the bounce shock, which can be seen in the lower Y_e , higher density, and higher infall velocities for model IPA outside the bounce shock (Figure 1) where the stronger IPA for low density does not shut off. This will increase the ram pressure as the shock passes through the Fe-core. The shock forms at $0.554 M_{\odot}$ in model IPA and $0.430 M_{\odot}$ in model Base, and the shallower shock launch results in a more vigorous launch of the shock for model IPA (Figure 9). Approximately 70 ms after bounce the shock trajectories of the two nuclear EC models cross (as reported by Hix et al. 2003) due to higher ram pressure from higher density and infall velocities in the outer core of model IPA induced by stronger deleptonization. The shock trajectories of models Base and IPA cross again late in our simulations, with the net effect that the shock position of model IPA is flatter during the epoch when we should expect multidimensional effects to become important. In the model using the B85 nucleon EC (Base-B85ea-np), the shock radius trails that in the Base model slightly, with the deficit reaching 5 km by the end of our simulations at 150 ms post-bounce. This deficit in shock radius for model Base-B85ea-np is reflected in an $\approx 2 \text{ Bethe s}^{-1}$ lower ν_e - and $\bar{\nu}_e$ -luminosity during the accretion phase relative to model Base, with a small (15 Bethe s^{-1}) decrease in the breakout ν_e -luminosity. The shallower bounce shock of model IPA also results in a breakout ν_e -luminosity burst that peaks sooner and higher (by $\approx 25 \text{ Bethe s}^{-1}$) than the LMSH EC model (Base), and then drops sooner creating a narrower breakout peak. Model IPA shows a higher $\nu_{\mu\tau}$ -luminosity from bounce to approximately 80 ms post-bounce.

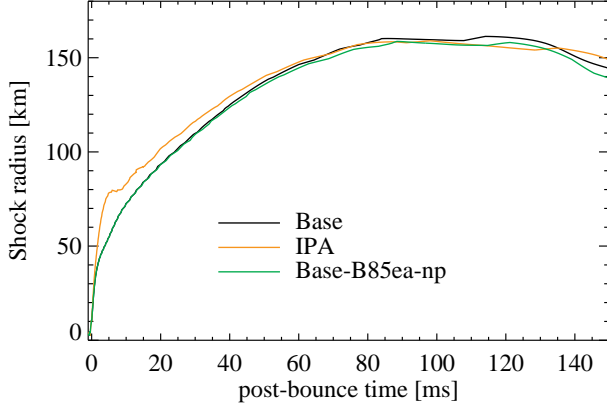


FIG. 9.— Shock trajectories in km, versus time after bounce, for all models in Section 3.2. Models are Base (black; all opacities), IPA (orange; IPA EC), and Base-B85ea-np (green; B85 EC on free nucleons).

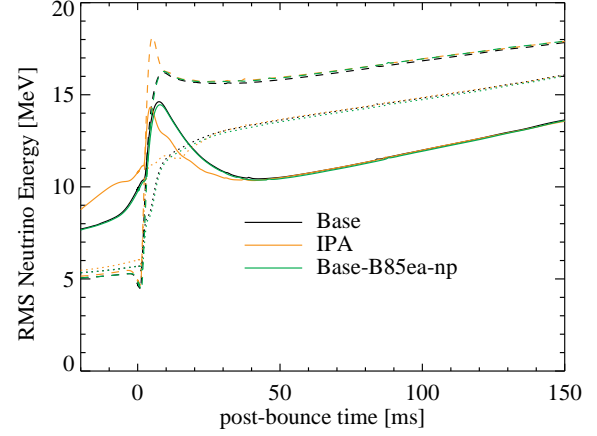


FIG. 11.— Comoving-frame neutrino RMS energies measured at 400 km for all models in Section 3.2. Colors are as in Figure 9. Line styles are as in Figure 3.

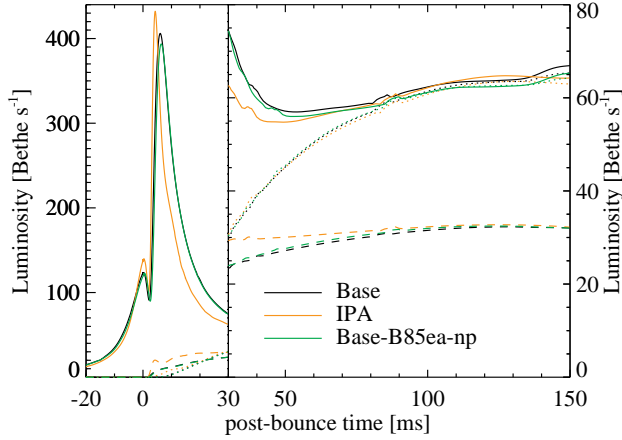


FIG. 10.— Comoving-frame neutrino luminosities measured at 400 km for all models in Section 3.2. Colors are as in Figure 9. Line styles are as in Figure 3. The luminosities are in Bethe s^{-1} , where 1 Bethe = 10^{51} ergs.

With no discernible differences in $\langle E_{\nu\mu\tau} \rangle_{\text{RMS}}$ outside the narrow peak during breakout (Figure 11), the higher luminosity of model Base-B85ea-np implies it is emitting more $\nu_{\mu\tau}\bar{\nu}_{\mu\tau}$ pairs than the other models. The $\langle E_{\nu} \rangle_{\text{RMS}}$ for all models is essentially identical for each neutrino species during the accretion epoch, with sharper and narrower peaks for model IPA during breakout, owing to the shallower and rapidly moving shock. Before bounce, model IPA shows a 1–2 MeV higher $\langle E_{\nu_e} \rangle_{\text{RMS}}$, reflecting the shift of the high-energy tail seen in Figure 8 and discussed in Section 3.1.3.

3.3. Pair opacity comparisons

To test the effect of pair opacities on the supernova models, we compare the Base model to models omitting e^+e^- annihilation (Base-noEPpair), bremsstrahlung (Base-noBrems), and both (Base-noPair) pair sources. Without any pair sources model Base-noPair also lacks $\nu_{\mu\tau}\bar{\nu}_{\mu\tau}$. At bounce there are no distinguishable differences among these models, which is consistent with the lack of thermal e^+e^- pairs to annihilate and free nucleons for bremsstrahlung. The shock trajectories for the models with missing pair opacities begin to deviate from model Base approximately 40 ms after bounce (Figure 12), with the model Base-noEPpair shock extending to 183 km, the model Base-noBrems shock extending to 163 km, and the model Base-noPair shock extending to

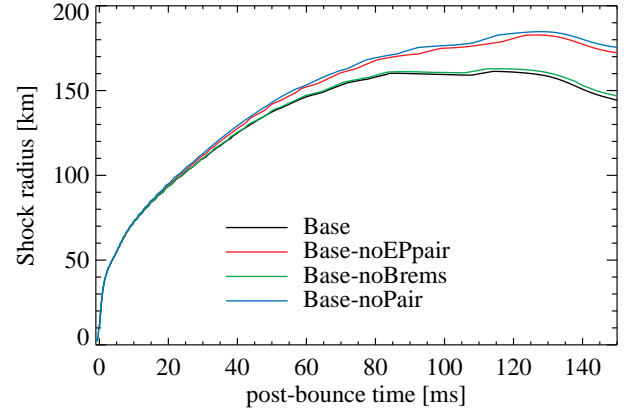


FIG. 12.— Shock trajectories in km, versus time after bounce, for the pair opacity test models in Section 3.3. The models are Base (black; all opacities), Base-noEPpair (red; without e^+e^- annihilation), Base-noBrems (green; without Bremsstrahlung), and Base-noPair (blue; without pair opacities).

185 km. These are the only models in this paper that exceed the maximum shock extent of the Base model at 161 km. (See Table 2.) Comparison of these models shows that e^+e^- annihilation is much more important to the shock propagation than bremsstrahlung.

Unlike the previous comparisons, where accretion-phase shock differences are correlated with ν_e - and $\bar{\nu}_e$ -luminosities, the luminosities (Figure 13) for these models are *anti-correlated* with the shock radii. The differences in the $\langle E_{\nu} \rangle_{\text{RMS}}$ for all neutrino species (Figure 14) are also anti-correlated, with the shock with smaller differences relative to model Base for model Base-noBrems and larger differences for model Base-noEPpair. In model Base-noPair the only source of ν_e is electron capture on protons and of $\bar{\nu}_e$ is positron capture on neutrons. As in the case of the EC–NIS interplay (Section 3.1.3), the non-linearity of pair opacity effects on the emission of $\nu_e\bar{\nu}_e$ is clear. For both luminosity and RMS energy the removal of bremsstrahlung had only a minor impact when e^+e^- annihilation was present. However, when e^+e^- annihilation was absent, the removal of bremsstrahlung had a significant impact on both.

Previous studies (Thompson et al. 2000, 2003; Burrows et al. 2000; Keil et al. 2003; Buras et al. 2003,

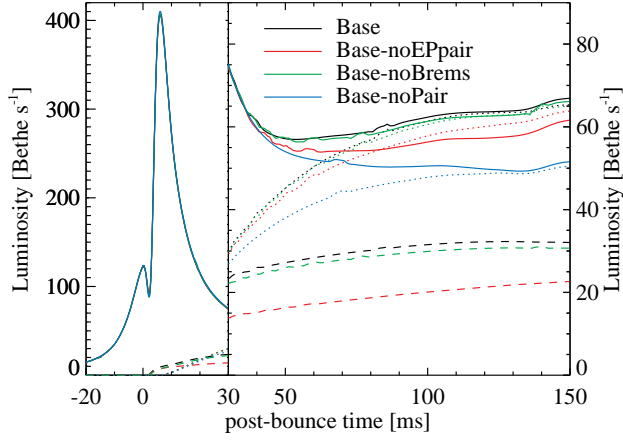


FIG. 13.— Comoving-frame neutrino luminosities measured at 400 km for all models in Section 3.3. Colors are as in Figure 12. Line styles are as in Figure 3. The luminosities are in Bethe s^{-1} , where 1 $\text{Bethe} = 10^{51}$ ergs. The dashed line for model Base-noPair $L_{\nu_{\mu\tau}}$ is omitted as this model does not include $\nu_{\mu\tau}\bar{\nu}_{\mu\tau}$.

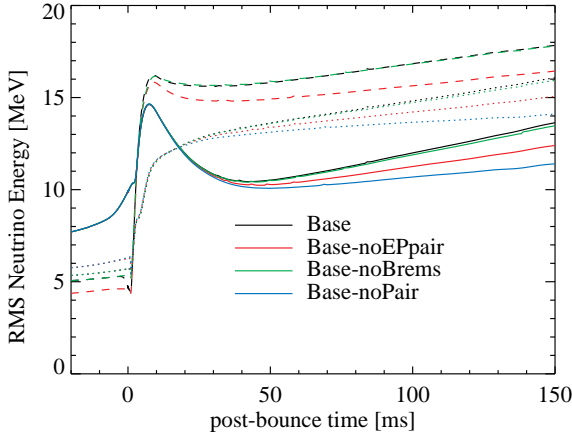


FIG. 14.— Comoving-frame neutrino RMS energies measured at 400 km for all models in Section 3.3. Colors are as in Figure 12. Line styles are as in Figure 3.

2006) have stressed the importance of bremsstrahlung as a neutrino-pair source. Buras et al. (2006) plotted (see their Figures 21–22) each opacity for all neutrino species at two energies for two post-bounce epochs within our study range and found that bremsstrahlung was the dominant pair-source in the proto-neutron star, but e^+e^- annihilation became dominant starting somewhere outside the neutrinosphere in each case. The $\nu_{\mu\tau}\bar{\nu}_{\mu\tau}$ emission rates for our models are consistent with that finding, being higher in the inner core for the bremsstrahlung-including models (Base, Base-noEPpair) than the model without bremsstrahlung (Base-noBrems). Stationary transport studies (Thompson et al. 2000; Burrows et al. 2000; Keil et al. 2003) have found bremsstrahlung to be more important than e^+e^- annihilation to the emitted flux and thermalization rate of $\nu_{\mu\tau}\bar{\nu}_{\mu\tau}$. Stationary transport studies drive toward a global equilibrium that is never reached during the dynamic shock revival phase and can overemphasize the region below the neutrinospheres where bremsstrahlung is dominant. A more relevant comparison is with the dynamic models of Thompson et al. (2003) computed with and without bremsstrahlung like our models, though with different progenitor, base opacities, code, etc. Thompson et al. (2003) find that the total luminosity for all heavy lepton neutrinos,

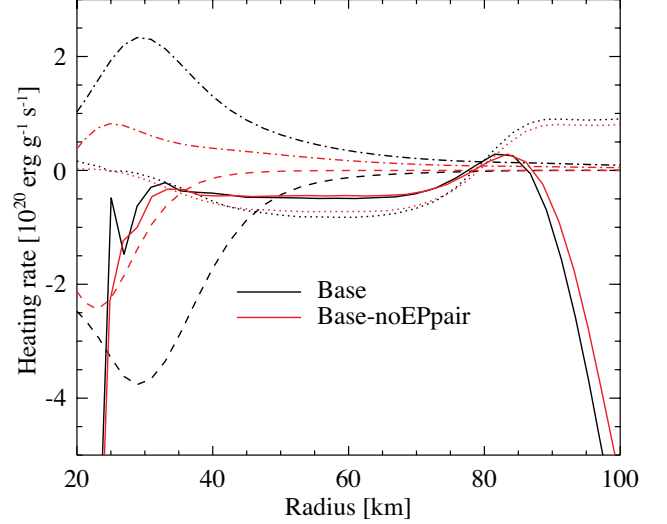


FIG. 15.— Net heating rates in $\text{ergs g}^{-1} \text{s}^{-1}$ for models Base (black) and Base-noEPpair (red) at 30 ms after bounce. Line styles indicate net heating by: emission/absorption by ν_e (solid) and $\bar{\nu}_e$ (dotted), by $\nu_{\mu\tau}\bar{\nu}_{\mu\tau}$ pair sources (dashed) and by NIS of $\nu_{\mu\tau}\bar{\nu}_{\mu\tau}$ (dash-dotted). Net pair heating for $\nu_e\bar{\nu}_e$ is approximately one order of magnitude or more smaller than the $\nu_{\mu\tau}\bar{\nu}_{\mu\tau}$ counterpart and is omitted from this plot for clarity.

$L_x = 2L_{\nu_{\mu\tau}} + 2L_{\bar{\nu}_{\mu\tau}}$, increases by 8–10 Bethe s^{-1} starting from about 30 ms after bounce onward. Our models are consistent with this change, showing an increase of 2 Bethe s^{-1} for each of the four heavy lepton (anti)neutrino species during the same epoch. The proportionate increase due to adding bremsstrahlung does appear larger for the Thompson et al. (2003) models as their model without bremsstrahlung has roughly half the neutrino luminosity for each species as our Base-noBrems model. Much of the difference can be attributed to our use of nucleon NIS and GR with the rest due to other differences between the opacities, progenitors, and codes. At later epochs, beyond the effective use of spherical models, the diffusion of core $\nu_{\mu\tau}\bar{\nu}_{\mu\tau}$ to the neutrinospheres may enhance the relative contribution of bremsstrahlung to the luminosity.

Removing pair sources reduces cooling by $\nu_{\mu\tau}\bar{\nu}_{\mu\tau}$ emission during the accretion phase. Figure 15 shows the net heating rate for models Base and Base-noEPpair at 30 ms after bounce, with the net cooling for $\nu_{\mu\tau}\bar{\nu}_{\mu\tau}$ emission shown as dashed lines. For the Base model, the cooling by $\nu_{\mu\tau}\bar{\nu}_{\mu\tau}$ emission dominates the radiative heat budget between 25 and 40 km, with about half of the cooling returned back to the local thermal pool by NIS on $\nu_{\mu\tau}\bar{\nu}_{\mu\tau}$. (In both of these models the full set of NIS opacities are available for thermalization during scattering.) When e^+e^- -annihilation is removed (Base-noEPpair, red lines), both the pair cooling and related NIS heating are reduced and shifted deeper into the core. The lower effective cooling by $\nu_{\mu\tau}\bar{\nu}_{\mu\tau}$ -pairs in model Base-noEPpair results in more thermal energy being available to support the shock and a larger shock radius. Emission of $\nu_e\bar{\nu}_e$ -pairs is suppressed by the largely filled ν_e phase space.

4. CONCLUSIONS

In this paper we have systematically examined the effects of each of the updated opacities in our modernized opacity set over the initial 150 ms post-bounce, spherically symmetric phase of core-collapse supernovae. To summarize our primary findings: (1) During collapse, electron capture on heavy nuclei dominates the emission of neutrinos and the delep-

tonization of the core. If modern EC rates are used with a detailed NSE composition, as in LMSH or Juodagalvis et al. (2010), the direct emission of low-energy neutrinos obviates the need for NES to fill the low-energy portion of the neutrino spectrum. (2) Omitting NES results in an $\approx 15\%$ increase in the breakout-burst ν_e -luminosity. (3) Changes in shock formation due to deleptonization are the primary opacity-driven source of variation in early shock evolution. (4) During the accretion phase, nucleon NIS enhances the $\nu_e\bar{\nu}_e$ -luminosities, net heating, and drives the shock further out, enhancing the potential of shock revival by multidimensional effects. (5) Cooling by $\nu_{\mu\tau}\bar{\nu}_{\mu\tau}$ -pair emission from e^+e^- -annihilation removes energy from the system that could otherwise be used to revive the shock. (6) All of the NIS opacities (except scattering on positrons) and e^+e^- -annihilation affect the neutrino luminosities and/or $\langle E_\nu \rangle_{\text{RMS}}$ during accretion. (7) Positron scattering shows no impact on the outcome or observables during our simulations.

We have identified non-linear behaviors in the interplay among opacities, which illustrate that the context provided by the included opacities is important in evaluating individual opacities. Some examples of neutrino opacity interplay include:

- Emission from nuclear EC and energy downscattering by NES compete to fill the lowest energy bins during collapse. The escape of low-energy ν_e increases core deleptonization. The low-energy spectrum of neutrinos emitted by the LMSH EC table fills the low-energy phase space adequately without NES; thus, we do not see an impact on deleptonization when NES is omitted as we do in the case of models using the IPA EC, which does not fill this part of the spectrum directly.
- Thermalization of $\nu_{\mu\tau}\bar{\nu}_{\mu\tau}$ by individual NIS opacities is not simply additive. Removing either NES or nucleon NIS results in a modest increase in $\langle E_{\nu_{\mu\tau}} \rangle_{\text{RMS}}$, while removing both results in a much larger increase, as thermalization by scattering above the emission region is absent.
- Neutrino emission by pair sources also exhibits saturation effects. In models including e^+e^- annihilation, bremsstrahlung has only a minor impact on the emitted neutrino properties, but when bremsstrahlung is the only pair source, its removal has a much larger impact.

We can identify from our tested set necessary neutrino-matter interactions required for modern supernova modeling in any dimension.

- Modern nuclear EC (LMSH, Juodagalvis et al. 2010, or equivalent) should be considered an essential ingredient in any realistic supernova simulation as was previously noted by Hix et al. (2003). Relying on the IPA EC artificially alters the electron capture, deleptonization, and the impact of other opacities.
- Nucleon NIS extends the shock radius via an increase in $\nu_e\bar{\nu}_e$ -luminosity. The related enhancements to capture on free nucleons, though relatively modest in effect, should be included for physical consistency of the nucleon opacities.
- NES significantly reduces ν_e emission during breakout and contributes to thermalizing the $\nu_{\mu\tau}\bar{\nu}_{\mu\tau}$ spectra.
- $\nu_{\mu\tau}\bar{\nu}_{\mu\tau}$ -pair emission by e^+e^- -annihilation is an important source of cooling during the accretion phase, while bremsstrahlung plays only a small role (as also seen in Thompson et al. 2003) unless e^+e^- -annihilation is omitted. Bremsstrahlung may become more important at later epochs as trapped $\nu_{\mu\tau}\bar{\nu}_{\mu\tau}$ diffuse out.

Omitting any of these opacities would alter the observable neutrino properties, and thus would introduce unnecessary systematic errors in the analysis of observed supernova neutrino signals.

The modern opacities discussed in this paper are physically well-motivated improvements to the reference Bruenn (1985) opacity set. Including these improved opacities increases the physical fidelity of the neutrino-matter interactions in supernova simulations, while omitting them risks potential systematic errors in the dynamical and observational properties of simulated supernovae.

E.J.L. received support from the NASA Astrophysics Theory and Fundamental Physics Program (grant number NNH11AQ72I) and the NSF PetaApps Program (grant number OCI-0749242). A.M. and W.R.H. are supported by the Department of Energy Office of Nuclear Physics; and A.M. and O.E.B.M. received support from the Department of Energy Office of Advanced Scientific Computing Research. This research was also supported in part by the National Science Foundation through TeraGrid resources provided by National Institute for Computational Sciences under grant number TG-MCA08X010. This research used resources of the Oak Ridge Leadership Computing Facility at the Oak Ridge National Laboratory, which is supported by the Office of Science of the U.S. Department of Energy under Contract No. DE-AC05-00OR22725.

REFERENCES

- Arnett, W. D. 1966, *Can. J. Phys.*, 44, 2553
 Arnett, W. D. 1977, *ApJ*, 218, 815
 Bludman, S. A., & van Riper, K. A. 1978, *ApJ*, 224, 631
 Bowers, R. L., & Wilson, J. R. 1982, *ApJS*, 50, 115
 Bruenn, S. W. 1975, in *Annals of the New York Academy of Sciences*, Vol. 262, Seventh Texas Symposium on Relativistic Astrophysics, ed. P. G. Bergman, E. J. Fenyves, & L. Motz, 80–94
 Bruenn, S. W. 1985, *ApJS*, 58, 771
 Bruenn, S. W., Dirck, C. J., Mezzacappa, A., et al. 2006, *J. Phys.: Conf. Ser.*, 46, 393
 Bruenn, S. W., & Haxton, W. C. 1991, *ApJ*, 376, 678
 Buras, R., Janka, H., Keil, M. T., Raffelt, G. G., & Rampp, M. 2003, *ApJ*, 587, 320
 Buras, R., Rampp, M., Janka, H.-T., & Kifonidis, K. 2006, *A&A*, 447, 1049
 Burrows, A. 2001, *Prog. Part. Nucl. Phys.*, 46, 59
 Burrows, A., & Sawyer, R. F. 1998, *Phys. Rev. C*, 58, 554
 Burrows, A., Young, T., Pinto, P., Eastman, R., & Thompson, T. A. 2000, *ApJ*, 539, 865
 Colgate, S. A., & White, R. H. 1966, *ApJ*, 143, 626
 Cooperstein, J., van den Horn, L. J., & Baron, E. A. 1986, *ApJ*, 309, 653
 Fischer, T., Whitehouse, S. C., Mezzacappa, A., Thielemann, F.-K., & Liebendörfer, M. 2010, *A&A*, 517, A80
 Fuller, G. M. 1982, *ApJ*, 252, 741
 Glashow, S. 1961, *Nucl. Phys. A*, 22, 579
 Hannestad, S., & Raffelt, G. 1998, *ApJ*, 507, 339
 Hasert, F. J., et al. 1973, *Phys. Lett. B*, 46, 138
 Hillebrandt, W., Nomoto, K., & Wolff, R. 1984, *A&A*, 133, 175

- Hix, W. R., Messer, O. E. B., Mezzacappa, A., et al. 2003, *Phys. Rev. Lett.*, 91, 201102
- Horowitz, C. J. 1997, *Phys. Rev. D*, 55, 4577
- Horowitz, C. J. 2002, *Phys. Rev. D*, 65, 43001
- Itoh, N., Asahara, R., Tomizawa, N., Wanajo, S., & Nozawa, S. 2004, *ApJ*, 611, 1041
- Juodagalvis, A., Langanke, K., Hix, W. R., Martínez-Pinedo, G., & Sampaio, J. M. 2010, *Nucl. Phys. A*, 848, 454
- Keil, M. T., Raffelt, G. G., & Janka, H.-T. 2003, *ApJ*, 590, 971
- Kodama, K., et al. 2001, *Phys. Lett. B*, 504, 218, (DONUT Collaboration)
- Lamb, D. Q., & Pethick, C. J. 1976, *ApJ*, 209, L77
- Langanke, K., & Martínez-Pinedo, G. 2000, *Nucl. Phys. A*, 673, 481
- Langanke, K., Martínez-Pinedo, G., Müller, B., et al. 2008, *Physical Review Letters*, 100, 011101
- Langanke, K., Martínez-Pinedo, G., Sampaio, J. M., et al. 2003, *Phys. Rev. Lett.*, 90, 241102
- Lattimer, J., & Swesty, F. D. 1991, *Nucl. Phys. A*, 535, 331
- Lentz, E. J., Hix, W. R., Baird, M. L., Messer, O. E. B., & Mezzacappa, A. 2010, in *Proceedings of Nuclei in the Cosmos XI*, ed. G. Martínez-Pinedo & et al. (SISSA Proceedings of Science), 152
- Lentz, E. J., Mezzacappa, A., Messer, O. E. B., et al. 2012, *ApJ*, 747, 73
- Liebdörfer, M., Messer, O. E. B., Mezzacappa, A., et al. 2004, *ApJS*, 150, 263
- Liebdörfer, M., Rampp, M., Janka, H.-T., & Mezzacappa, A. 2005, *ApJ*, 620, 840
- Liebdörfer, M., Rosswog, S., & Thielemann, F.-K. 2002, *ApJS*, 141, 229
- Marek, A., Janka, H.-T., Buras, R., Liebdörfer, M., & Rampp, M. 2005, *A&A*, 443, 201
- Martínez-Pinedo, G., Fischer, T., Lohs, A., & Huther, L. 2012, *Phys. Rev. Lett.*, submitted, (arXiv:1205.2793)
- Messer, O. E. B., Liebdörfer, M., Hix, W. R., Mezzacappa, A., & Bruenn, S. W. 2003, in *From Twilight to Highlight: The Physics of Supernovae*, ed. W. Hillebrandt & B. Leibundgut, *ESO Astrophysics Symposia* (Heidelberg: Springer), 70
- Mezzacappa, A., & Bruenn, S. W. 1993a, *ApJ*, 405, 669
- Mezzacappa, A., & Bruenn, S. W. 1993b, *ApJ*, 410, 740
- Mezzacappa, A., & Messer, O. E. B. 1999, *J. Comp. Appl. Math.*, 109, 281
- Müller, B., Janka, H.-T., & Marek, A. 2012, *ApJ*, 756, 84
- Myra, E. S., Bludman, S. A., Hoffman, Y., et al. 1987, *ApJ*, 318, 744
- Perl, M. L., Abrams, G. S., Boyarski, A. M., et al. 1975, *Phys. Rev. Lett.*, 35, 1489
- Reddy, S., Prakash, M., & Lattimer, J. M. 1998, *Phys. Rev. D*, 58, 013009
- Reddy, S., Prakash, M., Lattimer, J. M., & Pons, J. A. 1999, *Phys. Rev. C*, 59, 2888
- Roberts, L. F., & Reddy, S. 2012, *Phys. Rev. C*, submitted, arXiv:1205.4066
- Salam, A. 1968, in *Proc. of 8th Nobel Symposium*, ed. N. Svartholm (Stockholm: Almquist and Wiksells)
- Sampaio, J. M., Langanke, K., Martínez-Pinedo, G., & Dean, D. J. 2002, *Phys. Lett. B*, 529, 19
- Schinder, P. J., & Shapiro, S. L. 1982, *ApJS*, 50, 23
- Shlomo, S., Kolomietz, V. M., & Colò, G. 2006, *Eur. Phys. J. A*, 30, 23
- Smit, J. M., Cernohorsky, J., van den Horn, L. J., & van Weert, C. G. 1996, *ApJ*, 460, 895
- Swesty, F. D., Lattimer, J. M., & Myra, E. S. 1994, *ApJ*, 425, 195
- Thompson, T. A., Burrows, A., & Horvath, J. E. 2000, *Phys. Rev. C*, 62, 035802
- Thompson, T. A., Burrows, A., & Pinto, P. A. 2003, *ApJ*, 592, 434
- Tubbs, D. L., & Schramm, D. N. 1975, *ApJ*, 201, 467
- Weinberg, S. 1967, *Phys. Rev. Lett.*, 19, 1264
- Woosley, S. E., & Heger, A. 2007, *Phys. Rep.*, 442, 269
- Yahil, A. 1983, *ApJ*, 265, 1047
- Yamada, S., Janka, H.-T., & Suzuki, H. 1999, *A&A*, 344, 533
- Yueh, W. R., & Buchler, J. R. 1976, *Ap&SS*, 41, 221